

Article

Evaluation of Sulfide Control by Air-Injection in Sewer Force Mains: Field and Laboratory Study

Juan T. García *, Antonio Viguera-Rodríguez, Luis G. Castillo and José M. Carrillo

Hidr@m Group, Department of Civil Engineering, Universidad Politécnica de Cartagena, Paseo Alfonso XIII, 52, 30203 Cartagena, Spain; aviguera.rodriguez@upct.es (A.V.-R.); luis.castillo@upct.es (L.G.C.); jose.carrillo@upct.es (J.M.C.)

* Correspondence: juan.gbermejo@upct.es; Tel.: +34-968-327-026; Fax: +34-968-325-435

Academic Editor: Vincenzo Torretta

Received: 1 January 2017; Accepted: 2 March 2017; Published: 8 March 2017

Abstract: Chemical and biological processes consume dissolved oxygen (DO) in urban wastewater during transportation along sewer systems. Anaerobic conditions ($DO < 0.2$ mg/L) are easily reached, leading to sulfide (S^{2-}) generation. Release of free sulfide, hydrogen sulfide gas (H_2S), from the liquid to the gaseous phase, causes odor, corrosion of pipes and supposes a risk for health of people working in sewers. These issues get worse in force mains, due to inability to take oxygen from the gaseous phase of pipe. Air injection is a suggested practice to control H_2S emission in force mains. That technique aims to keep aerobic conditions in wastewater in order to avoid sulfide generation and favor a decrease of Biochemical Organic Demand (BOD). However, several force mains with air injection are not achieving their goals due to a limited oxygen transfer. Field measurements of dissolved oxygen in urban wastewater are presented in an existing force main with air injection during the summer of 2014 in the southeast of Spain. A laboratory scale model is constructed to quantify two-phase flow conditions in pipe due to air injection for different incoming flows rates of water and air. Particularly, for the case of plug flow, also known as elongated bubble flow. Velocity field measurement of water phase in laboratory allows estimating turbulent diffusivity of oxygen in the water, E_m , and inter-phase mass transfer coefficient $K_L(T)$. In the laboratory, flow and air depth, bubble length, water velocity field, pressure inside force main and water and airflow rates are determined experimentally. These variables are used to assess DO in water phase of force main by comparison with those obtained from field measurements. This work allows assessing air injection efficiency in wastewater, and, therefore, to predict DO in wastewater in force mains.

Keywords: air injection; force main; sewer system; hydrogen sulfide; two-phase flow; interphase mass transfer; turbulent diffusivity

1. Introduction

Air injection in force mains is a suggested practice to control H_2S emission [1,2], and has been used in several pump stations from 1942 in California. Pomeroy compared measurements of sulfide in liquid phase of wastewater in six force mains whose diameters varied from 0.2 to 1.3 m, with and without air injection [3]. Nevertheless, the work does not present systematic measurements and lacks of some information such as wastewater flow rate, retention time, slope of the pipes, or input and output BOD values. Reduction of H_2S is high for most of the cases including air injection. Recommendations for required airflow rates were given based only on pipe diameter. In 1974, EPA [4] presented measurements in the city of Texas in two force main with low input values of dissolved sulfide, around 2–3 mg/L, and retention time below 1 h. In that study, significant efficiencies are achieved for air–water ratios ranging from 25% to 40% and an air injection from 0.17 to 0.23 m³/h per mm of pipe inner diameter. The study cannot be reproduced as it lacks relevant prototype data such as

the operating time of pumps per day. Afterwards, EPA published a design manual [5] that includes Pomeroy's rule of thumb [3] to define the air injection flow rate, and a proposal taking into account water and air velocities, pressure of the main and rate of consumed oxygen.

Tanaka and Takenaka [6] experimented in prototype in the city of Kobe, Japan, with 350 mm of diameter, 3640 m length and slope of 1.4%. Retention time ranged from 4 to 7.5 h, with comprehensive measures of input and output sulfide in liquid, H_2S released to phase gas at the output, temperature, ratio of air–water flow rate and retention time. Good efficiencies are reached for air–water ratios range over 50% in seasons with higher temperatures, where sulfides are around 0.2 mg/L and H_2S in atmosphere is under 10 ppm. Authors proposed an equation to calculate the airflow rate that depends on the dissolved Chemical Organic Demand (CODs), the Hydraulic Retention Time (HRT) and DO at terminal and pump station points. Conditions of two-phase flow such as height of wastewater and air, contact surface, flow type (stratified, multi-bubble airflow, etc.), are not clarified, referring to other works [7,8] to calculate head losses due to air injection.

In Figure 1, the different airflow rates proposed are presented for the case of a pipe of 700 mm diameter—the size of the prototype tested in this work—and different water flow rates.

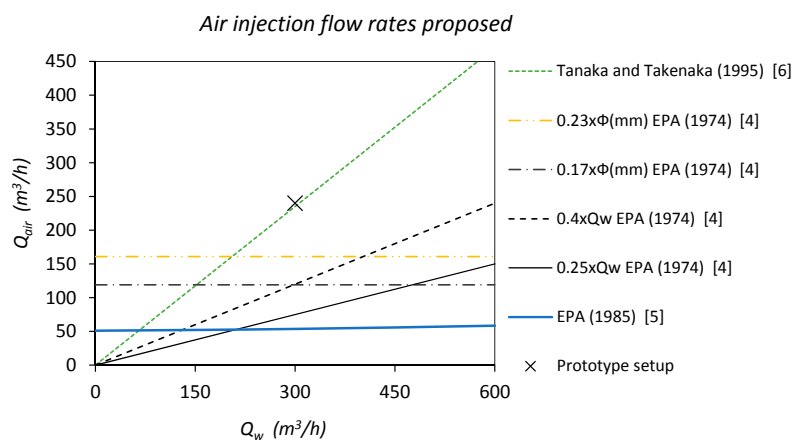


Figure 1. Airflow rate proposed by different researchers to avoid sulfide generation for case of pipe of 700 mm diameter. Airflow rate expressed in normal conditions, 1 atm and 20 °C.

Ochi et al. [9] carried out experiments in a laboratory physical device consisting of a 100 mm diameter 900 m long pipe in which they compared cases with and without air injection. The wastewater was stored in a tank during a period of 2 h to adjust the dissolved oxygen and the redox potential to field conditions. The air–water injection ratio, Q_a/Q_w , was in the range of 21%–42%, whereas water velocity was between 0.3 and 0.6 m/s. Dissolved sulfides measured with air injection were very low at the outlet, which verifies injection efficiency, in contrast with non-injection tests. From experimental data, the balance of oxygen in the liquid phase is established. The rate of oxygen uptake from the gaseous phase, R_f , is adjusted through an empirical equation similar to the one presented in the EPA design Manual [5].

Tanaka et al. [10] presented a work performed in a pressure sewer in Kawasaki, Japan. Inner diameter and length were 349 mm and 3500 m, respectively, and slope was around 0.3%. Air–water ratio was from 7% to 47%, wastewater velocity from 0.18 to 0.26 m/s, and oxygen transfer velocity in the interphase at 20 °C, $K_L(20)$, between 0.19 and 0.32 m/h for wastewater velocities of 0.3 and 0.6 m/s, respectively. Measurements verified that air injection was efficient to control sulfide generation and high levels of dissolved oxygen, 2–4 mg/L are reached. Two-phase flow conditions, height of wastewater and air, were calculated by a hydraulic model of two-phase flow proposed [7,8].

Two-phase flow in a pipe, considered as one-dimensional, has been extensively studied [11,12]. Figure 2 shows flow pattern for case of quasi-horizontal pipes with upward sloping depending on surface water velocity, u_{SL} , and surface gas velocity u_{SG} , which are defined by dividing water and

airflow rate by the pipe area, respectively [13,14]. Values that appear in Figure 2 correspond to the flow rates tested in a scale model built with Froude similarity to the field conditions. Pump stations of sewer systems usually work in the pattern named elongated bubble flow or plug flow. This flow is between slug flow and stratified flow.

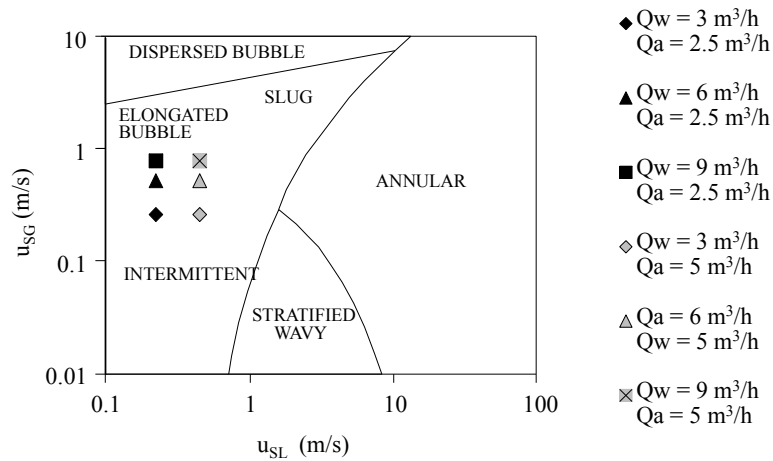


Figure 2. Flow pattern of two-phase flow upward sloping [13,14].

Plug flow is an intermittent bubbly flow, in which there is an important mass exchange between air and liquid phase fundamentally at the front and back part of each bubble (Figure 3). Thus, quantify frequency of bubbles is an important parameter to quantify oxygen transfer velocity in the interphase surface, $K_L(T)$. Actually, in the stratified flow, which consists in a continuous bubble, the mass transfer decreases considerably respect to plug or slug patterns due to the inexistence of back and front parts of the bubble.

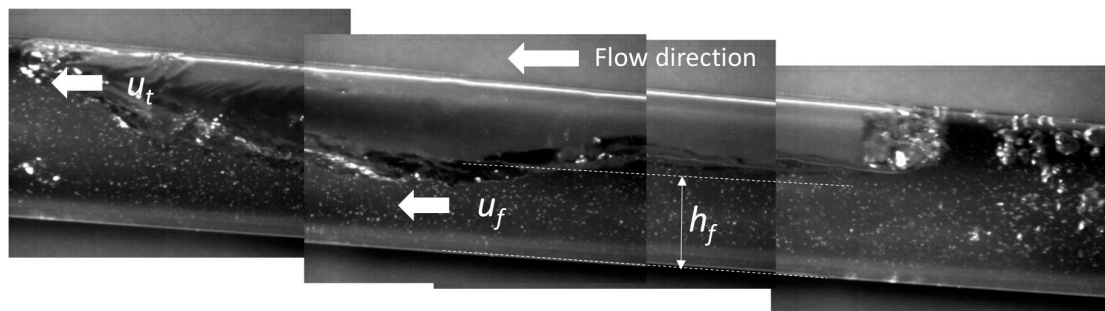


Figure 3. View of elongated bubble flow (plug flow) in the laboratory scale model.

To distinguish plug flow from slug flow, it is commonly used the criterion of the Froude number square of a two-phase flow, F_{R2}^2 , higher than 1.2, presented in Equation (1):

$$F_{R2}^2 = \frac{(u_t - u_f)^2}{g\Phi} > 1.2 \quad (1)$$

where u_i is the velocity at the top part of the bubble (m/s); u_f is the velocity below the bubble (m/s) as seen in Figure 3; Φ is the diameter of the pipe (m); and g is the gravity acceleration (m/s^2). In the case of slug flow, parameters such as flow depth in the bubble zone, h_f , and velocity values in the water and gas flow, can be obtained by momentum equations [14]. However, in elongated bubble flow, these parameters are not easily obtained by momentum equations due to flow complexity and should be measured in a physical device.

Air injection in a force main (prototype) located in the southeast of Spain was working inefficiently despite following the previous recommendations shown in Figure 1, where the prototype ratio is also represented.

In this paper, continuous DO field measurements in a force main of 700 mm inner diameter are presented. The H_2S concentrations in the atmosphere of the discharge manhole and other relevant variables are shown. Due to the previously mentioned inefficiency of the air injection in the prototype, a scale model was built. The scale model is used for characterizing the elongated bubble flow with regard to the oxygen transfer to the water. Velocity fields and flow depths measured in scale model are used to estimate interphase mass transfer coefficient, $K_L(T)$, as well as the turbulent diffusivity, E_m . Parting from these parameters the define oxygen transferred to water in the force main is calculated, being the results compared with field measurements of DO in the prototype.

2. Experimental Setting

2.1. Sewer Pumping Station

Field measurements were carried out in summer of 2014 in a force main whose pumping station is named “Las Gaviotas”. Such sewer system is located in La Manga (southeast of Spain), which is a town with a high seasonal to permanent population ratio. Force main length comes to 1500 m, lifting the wastewater from -0.90 to 15.75 m above sea level. The pipe is a high-density polyethylene with inner diameter 700 mm (Figure 4a). Instantaneous flow rates are around 1200 m^3/h and wastewater is being pumped during fifteen minutes per hour, so mean flow rate is 300 m^3/h . The flow rate of wastewater is measured by an electromagnetic flowmeter Endress Hauser Promag 50L-400 mm diameter. Air compressor is a Rotary Screw Compressor Ingersol Rand UP5 22 that pumps a maximum airflow rate of 240 m^3/h (Figure 4b), referred to normal conditions. The airflow rate is measured by a CS Instruments VA 420 Compressed Air Flow Meter of 20 mm diameter.

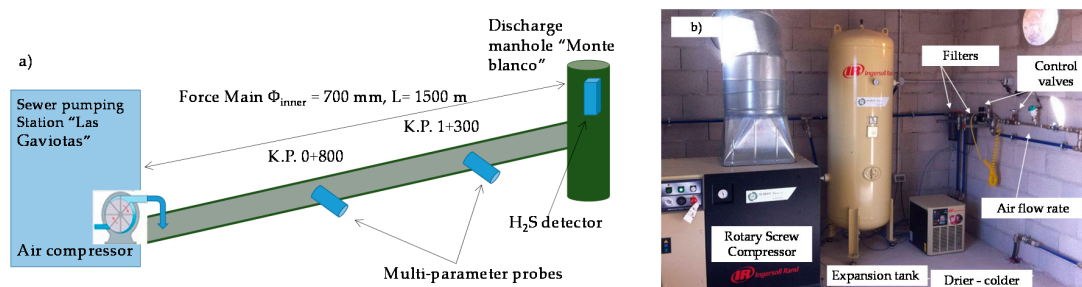


Figure 4. (a) Scheme of sewer pumping station; and (b) view of Air compression system.

Two multi-parameter probes HANNA HI 9828, that characterize physicochemical and electrical wastewater, were located at kilometric points (K.P.) 0 + 800 and 1 + 300 m, inside of the pipe (Figure 4a), i.e., 800m and 1300 m downstream the pumping station, respectively. The probes were located at a side of the pipe, 0.40 m below its upper point (Figure 5a,b).

During the prototype measurement campaign, the multi-parameter probes were used for registering dissolved oxygen in the wastewater (DO), oxidation reduction potential (ORP), electrical conductivity (EC), temperature (T), hydrogen potential (pH) and total dissolved Solids (TDS) at both points. At the discharge manhole of the main is located a Dräger X-am 5000 detector of H_2S concentrations in atmosphere.

Tests include periods in which air compressors were working whereas the sewer pumps were on or off (Table 1). Each combination was repeated at least once every eight days (A1–A8). At the location of the probes K.P. 0 + 800 and K.P. 1 + 300, the pipe slope is around 1% and 4%, respectively. Airflow rates are referred to the normal conditions of 1 atm and 20 $^{\circ}C$.

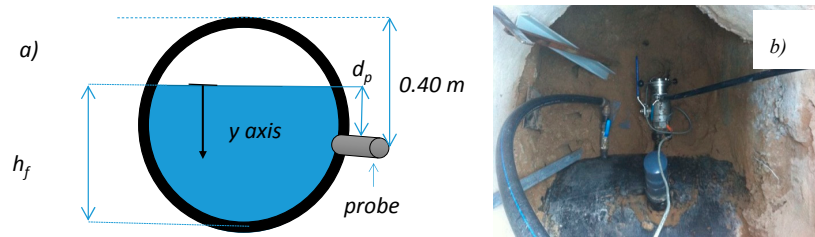


Figure 5. (a) Scheme of location of multi-parametrical probe in the force main; and (b) plan view of the location of the multi-parametrical probe at 0 + 800 m.

Table 1. Field-tests descriptions.

Pipe Slope	1%	4%	Test
Water flow rate (m ³ /h)	0; 1200	0; 1200	A1–A8
Airflow rate (m ³ /h)	240	240	

During the measurement campaign the temperature of wastewater was around 28 °C, the registered pressures were 2.8 and 2.5 bar in the 0 + 800 and 1 + 300 positions, respectively, and all the other variables were measured and registered with a sample frequency of 0.20 Hz.

2.2. Laboratory Scale Model

The model in the laboratory is a 1:10 scale model composed of a Plexiglas pipe with an inner diameter of 64 mm; a length of 6 m (as seen in Figure 6). The pipe slope can vary from 0% to 10%. Clear water with flow rates up to 10 m³/h is recirculated from two tanks with a total capacity of 3000 L. Air is injected at the beginning of the pipe by its upper part. Air-compressor injects air at a maximum flow rate of 5 m³/h. CS Instruments VA 420 Compressed Air Flow Meter of 15 mm diameter is installed to measure airflow. A rotameter water flow meter is in the liquid circuit. Liquid flow is registered by a high-speed camera to 1000 Hz. Images record a liquid flow that has been seeded with 100 µm polyamide particles.



Figure 6. View of the model in the hydraulic laboratory of the Universidad Politécnica of Cartagena (Spain).

Table 2 details tests comprising slopes of 1% and 4%; water flow rates of 0, 3, 6 and 9 m³/h; and airflow rates of 2.5 and 5 m³/h (B1–B16). Airflow rates are referred to the normal conditions of 1 atm and 20 °C.

Table 2. Laboratory tests descriptions.

Pipe Slope	1%	4%	Test
Water flow rate (m ³ /h)	0, 3, 6, 9	0, 3, 6, 9	B1–B16
Airflow rate (m ³ /h)	2.5, 5	2.5, 5	

3. Results and Discussion

3.1. Laboratory Scale Model

3.1.1. Velocity Field of Water Phase and Turbulent Diffusivity

Images recorded by a high speed camera Photron FASTCAM SA3 120k at 1000 Hz are analyzed in consecutive pairs by cross-correlation algorithm in interrogation areas of 20×20 pixel, single pass search and non-overlapping sub-windows [15]. Images are divided into four zones which are analyzed separately, obtaining an averaged velocity for each sub-division. These four zones are: (i) front part of the bubble; (ii) body of the bubble; (iii) back part of the bubble; and (iv) slug of water (Figure 7). This is due to the fact that each part registers significantly different velocity ranges. Recording time is about 1.5 minutes in which bubbles passing were analyzed. The PIVlab 1.41 software was used for the cross correlation. This program is an open source time resolved particle image velocimetry toolbox for Matlab [16].

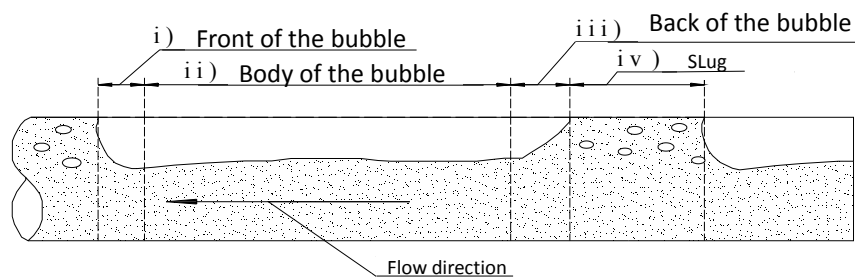


Figure 7. Detail of division of image to calculate velocity field by cross-correlation algorithm [15].

The velocity values of each of the four zones were time averaged and space averaged in each of the four parts in the way:

$$\bar{u}_{(x,y)} = \frac{\sum_{i=1}^j u_{(x,y,i)}}{j}; \bar{v}_{(x,y)} = \frac{\sum_{i=1}^j v_{(x,y,i)}}{j} \quad (2)$$

$$\bar{u} = \frac{\sum_{x=1}^m \sum_{y=1}^n \bar{u}_{(x,y)}}{m \times n}; \bar{v} = \frac{\sum_{x=1}^m \sum_{y=1}^n \bar{v}_{(x,y)}}{m \times n} \quad (3)$$

where $\bar{u}_{(x,y)}$, $\bar{v}_{(x,y)}$ are time averaged velocities in each sub-window of 20×20 pixel in each of the four parts of the image; x and y are the longitudinal and perpendicular coordinates, respectively; j is the number of pair of images averaged; \bar{u} , \bar{v} are the space averaged velocities of all sub-windows in each zone; and m and n are the indexes of the matrix sub-index which conform each of the four areas. Velocity fluctuations are also calculated from Equations (4) and (5):

$$u'_{(x,y)} = \sqrt{\frac{\sum_{i=1}^j (u_{(x,y,i)} - \bar{u}_{(x,y)})^2}{j}} \quad (4)$$

$$v'_{(x,y)} = \sqrt{\frac{\sum_{i=1}^j (v_{(x,y,i)} - \bar{v}_{(x,y)})^2}{j}} \quad (5)$$

where $(u_{(x,y,i)} - \bar{u}_{(x,y)})^2$, $(v_{(x,y,i)} - \bar{v}_{(x,y)})^2$ are the square of standard deviation of time averaged velocities in each sub-window for longitudinal and perpendicular directions. Equation (6) presents calculations of turbulent kinetic energy, $k(x, y)$:

$$k_{(x,y)} = \frac{u'^2_{(x,y)}}{2} + \frac{v'^2_{(x,y)}}{2} \quad (6)$$

From Equation (7) turbulent viscosity is calculated, as proposed in by Socolofsky and Jirka [17]. Assuming that turbulent Schmidt number adopts a value of unity, turbulent viscosity equals turbulent diffusivity, $E(x, y)$:

$$E_{(x,y)} \approx \sqrt{k_{(x,y)}} 0.07\Phi \quad (7)$$

where Φ is the inner diameter of the pipe. Finally, a spatial averaged value for the turbulent diffusivity for each one of the four zones is obtained by Equation (8):

$$E = \frac{\sum_{x=1}^m \sum_{y=1}^n E_{(x,y)}}{m \times n} \quad (8)$$

Figure 8 shows some of the results obtained by image analysis from Equations (2)–(8). Higher values of turbulent diffusivity, associated to greater oxygen transfer from air into water, are measured in the front and back zones of the bubble. As example in Figure 8, test “B10” shows a diffusivity of $3.55 \times 10^{-6} \text{ m}^2/\text{s}$ in the body of the bubble, whereas the diffusivity in the back zone rises to $1.13 \times 10^{-5} \text{ m}^2/\text{s}$.

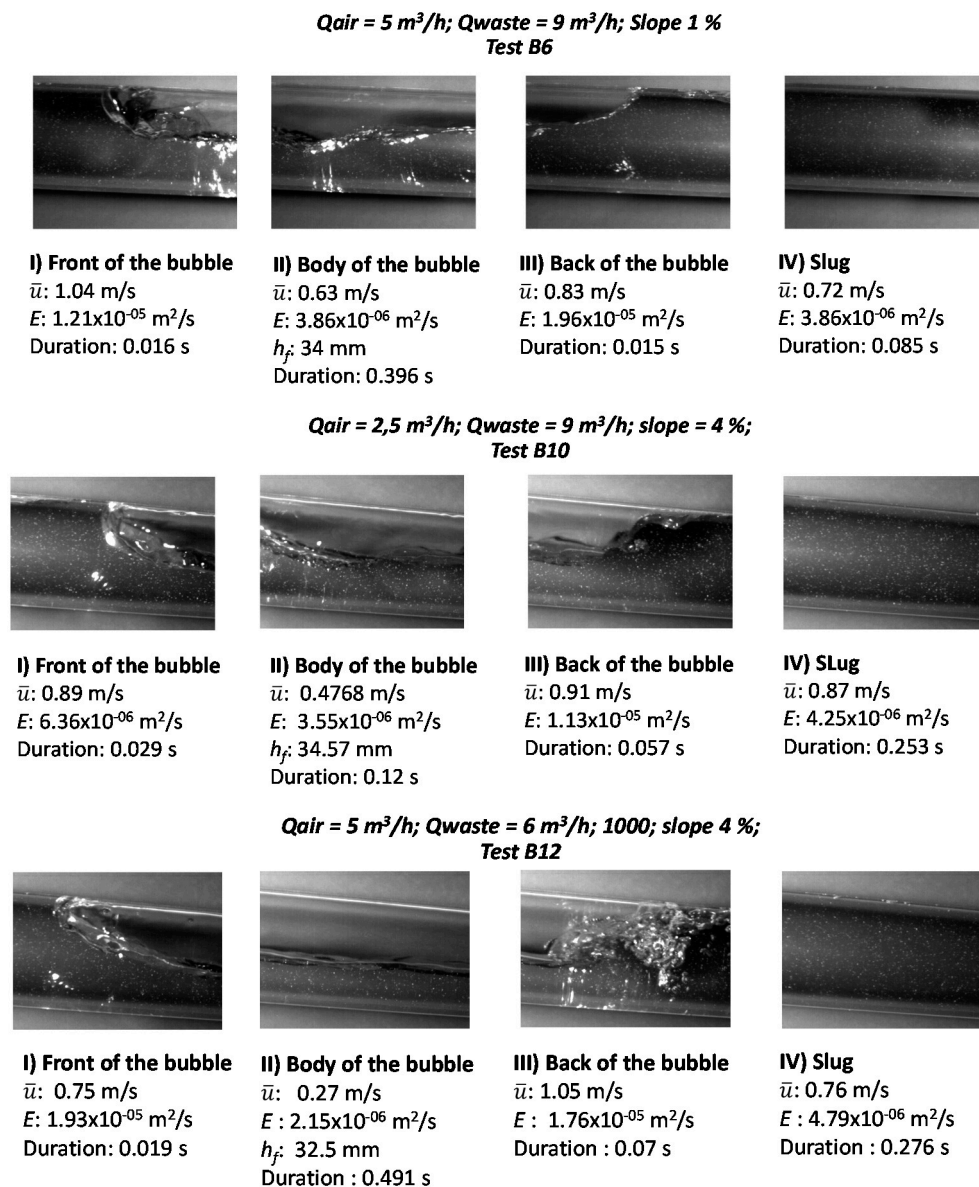


Figure 8. Cont.

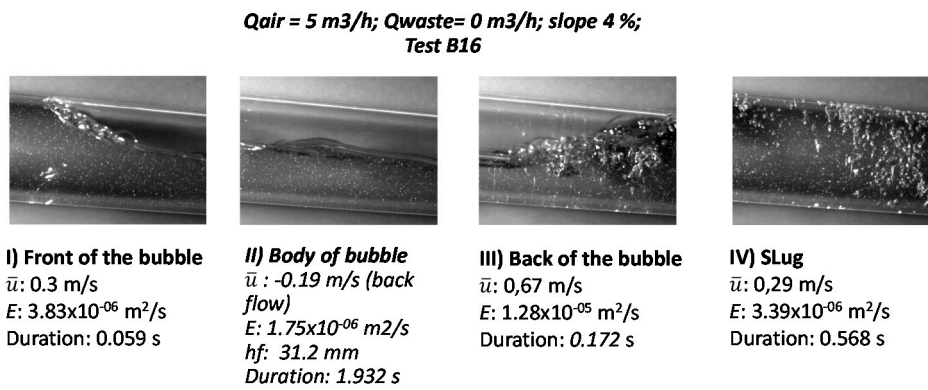


Figure 8. View of parameters calculated by time and spatial averaged in the four zones of the flow for tests B6, B10, B12 and B16.

Figure 9 shows the calculated turbulent diffusivity of all of the performed tests (B1–B16). Values show dependence on position more than the flow conditions. In the back zone of the bubble, turbulent diffusivity varies from 8.2×10^{-6} to $2.65 \times 10^{-5} \text{ m}^2/\text{s}$. Moreover, the bubble frequency has found to be of major relevance for mass transfer. In the case of a very long bubble, mass transfer will be less important than in the case of multiple bubbles. In fact, the time that lasts from the front to the back zone of the bubble is reduced with the bubble frequency. Figure 10a presents bubble duration for each slope and water flow rate. Such duration is used for calculating the time average turbulent diffusivity of the whole flow which is shown in Figure 9b. It can be seen the greater the water flow rate and slope, the greater the turbulence viscosity E_m .

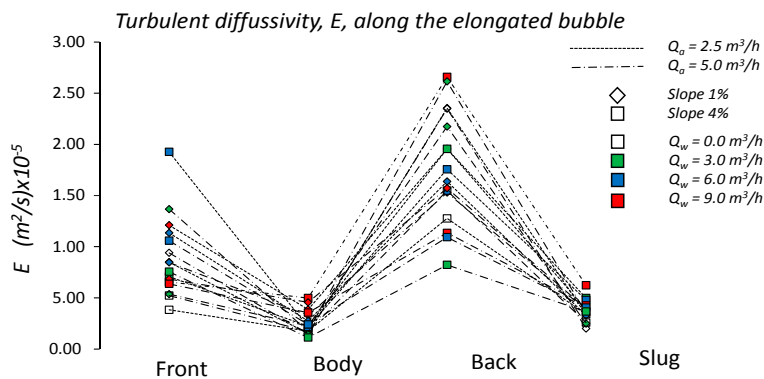


Figure 9. View of parameters calculated by time and spatial averaged in the four zones of the flow for tests B6, B10, B12 and B16.

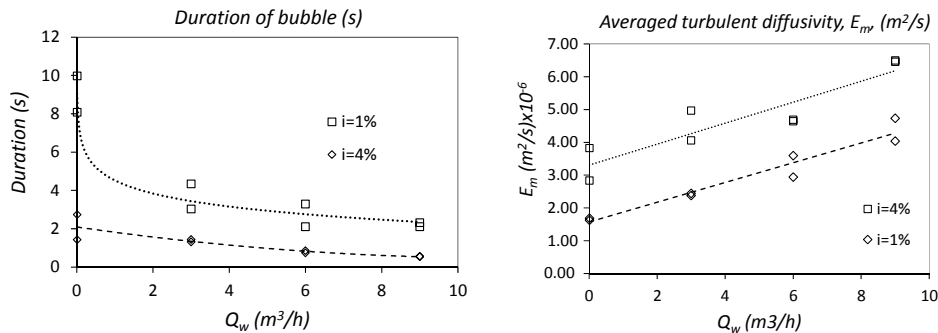


Figure 10. (a) Duration of bubble for each water flow rate and slope of the force main; and (b) turbulent diffusivity averaged for each water flow rate and slope.

3.1.2. Flow Depth in the Body of the Bubble, h_f

From experimental tests in laboratory scale model, B1–B16, elongated bubble flow parameters such as depth in the bubble zone, h_f , are measured. Therefore, Froude number square of two-phase flow, F_{R2}^2 , presented in Equation (1) can be calculated. Figure 11a presents values of h_f for several water flow rates and slopes. It can be seen how water depth decreases with slope, and increases with water flow rate. Figure 11b shows the dependence between the dimensionless water depth h_f/Φ and the two-phase Froude number square in the bubble zone. Moreover, two-phase Froude number square values are mostly below 1.2, verifying the two-phase pattern is elongated bubble flow instead of the slug flow pattern that is usually the dominant pattern in the literature.

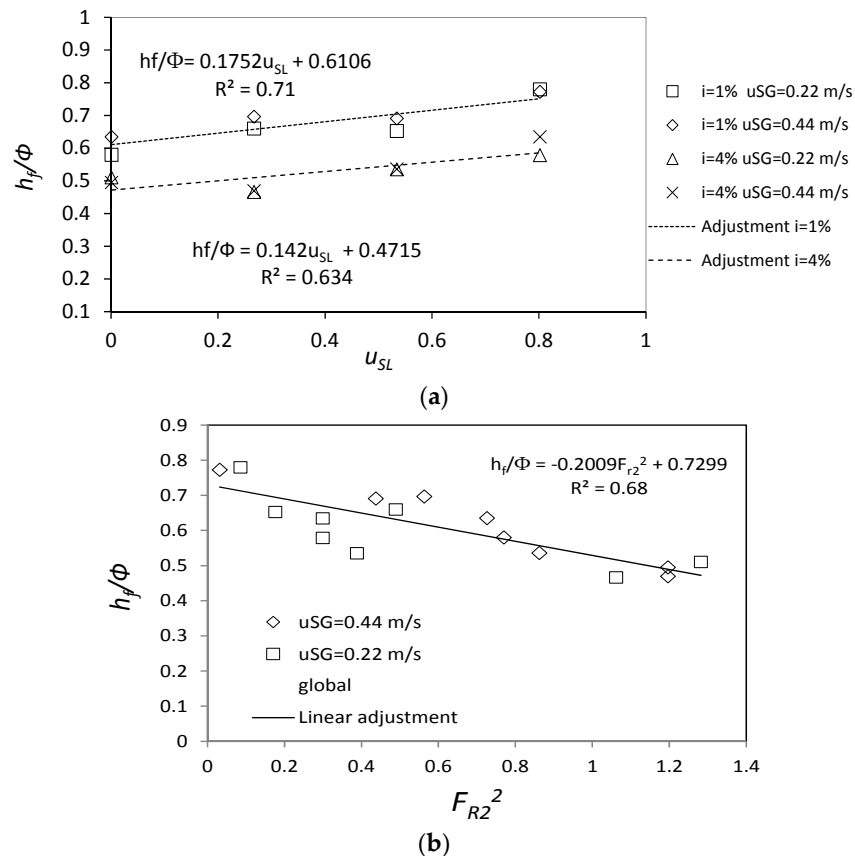


Figure 11. (a) Depth of the flow in the bubble body, h_f ; and (b) Froude number square of the bubble zone, F_{R2}^2 .

3.1.3. Linear Regression of the Turbulent Diffusion, E_m

Turbulent diffusivity, E_m , depends on surface flow velocity, u_{SL} , and both grow linearly. It also depends on slope of the pipe, i , and the depth of flow in the body of the bubble, h_f . A linear regression is proposed in Equation (9):

$$E_m \text{ adjusted} = 2.43 \times 10^{-6}F_r + 6.20 \times 10^{-5}i + 3.10 \times 10^{-6}\frac{h_f}{\Phi} - 8.29 \times 10^{-7} \quad (9)$$

where F_r is the wastewater Froude number, presented in Equation (10):

$$F_r = \frac{Q_w}{S_{force}\sqrt{g\Phi}} \quad (10)$$

The correlation coefficient of the fitting, shown in Figure 12, comes to 88%.

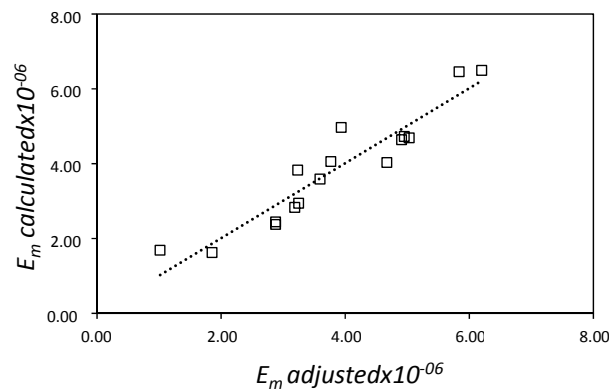


Figure 12. Linear regression of calculated E_m .

3.1.4. Mass Transfer Coefficient at the Air–Water Inter-Phase, $K_L(T)$

The interfacial transfer rate of low solubility gases is parameterized by the liquid phase gas transfer velocity or transfer coefficient $K_L(T)$, at the flow temperature, responding to first Fick's law, Equation (11):

$$J = K_L(T)(C_{sat} - C) \quad (11)$$

where J is the gas flux per unit interfacial area into or out of the water column. C_{sat} and C are the saturated and bulk concentration of dissolved air, respectively. In this inter-phase coefficient, we can distinguish two important zones: (i) the front and back part of the bubble; and (ii) the body of the bubble. The mass transfer in the inter-phase of the body of the bubble is calculated through experimental models [18] which consider transfer due to flow and air motion, $K_{Lw}(T)$ and $K_{Lair}(T)$, respectively. On the other hand, in the front and back zones of the bubble an important mixture of air and water is shown. Actually, in most cases, a major entrance of bubbles in the water phase come about as shown in Figures 3 and 7. Thus, inter-phase mass transfer in such zones can be based on experimental works about mass transfer from bubbles [19,20]. Those papers considered an averaged size of bubbles, air–water interface area and length of mixture, leading to a mass transfer coefficient $K_{Lbubble}(T)$. Details of above equations are included in the Appendix A. In order to calculate the mass transfer coefficient for the whole inter-phase, the following weighted average among the three values of inter-phase mass transfer is suggested:

$$K_L(T) = \frac{(K_{Lw}(T) + K_{Lair}(T))l_f S_w + (K_{Lbubble}(T))2l_{mixture} S_{force}}{(l_f S_w + l_{slug} S_{force})} \quad (12)$$

where l_f , $l_{mixture}$ and l_{slug} are the lengths of the elongated bubble, the slug of water after the bubble, and the mixing zone at the front and back part, respectively (m). S_w and S_{force} are the transversal surface occupied by water and total transversal surface of the pipe, respectively (m²). S_w is obtained as a function of the diameter of the pipe and the flow depth in the body of the bubble, h_f (see Section 3.1.2).

The length of elongated bubble increases when the slope and the water flow rate decreases. Measures and a fitting for each slope are presented in Figure 13.

The longer the length of bubble is, the less number of bubbles per unit time are, and therefore the less mass transfer by front and back zones are. Transfer coefficient is calculated through Equation (12) for test cases and presented in Figure 14. Different values are observed depending on the pipe slope, the water flow rate and the airflow rate. Airflow rate has been fixed in 2.5 and 5.0 m³/h in the tests, referred to normal conditions, showing that mass transfer is sensitive to water and airflow rate. A dimensional and sensitivity analysis has been carried out. Dimensionless group proposed includes three terms: the wastewater Froude number, F_r ; the ratio of airflow rate to water flow rate, Q_a/Q_w , and the Reynolds number of wastewater, R_e , presented in Equations (13) and (14) for slopes of 1% and

4%, respectively. The fitted model presented in Equations (13) and (14) shows a good agreement with the data (Figure 14).

$$\text{Slope} = 1\% \rightarrow K_L(T) = 3.0 \times 10^{-5} \left[Fr \left(\frac{Q_a}{Q_w} \right)^{0.3} + 3 \times 10^{-7} Re \right] + 5.0 \times 10^{-7} \quad (13)$$

$$\text{Slope} = 4\% \rightarrow K_L(T) = 4.5 \times 10^{-5} \left[Fr \left(\frac{Q_a}{Q_w} \right)^{0.3} + 3 \times 10^{-7} Re \right] + 3.0 \times 10^{-6} \quad (14)$$

being

$$Re = \frac{Q_w \Phi}{S_{force} \nu} \quad (15)$$

and where ν is the kinematic viscosity of water.

The adjusted dimensionless group considers two constants: an exponent 0.3 for the Q_a/Q_w factor, and a constant factor 3×10^{-7} that multiplies the Reynolds number. Results are presented in Figure 14.

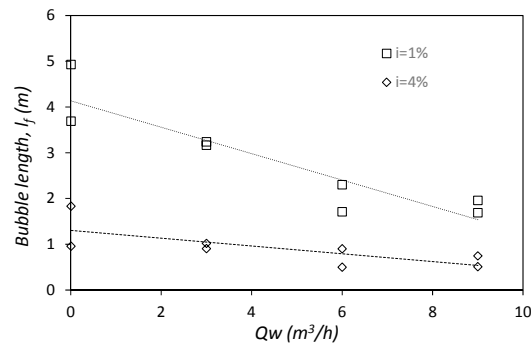


Figure 13. Bubble length measured for each water flow rate in function on the pipe slope.

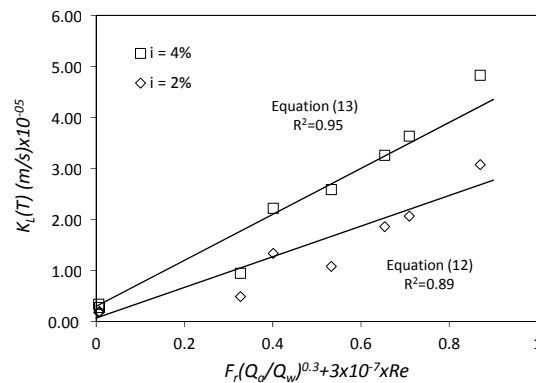


Figure 14. Mass transfer, $K_L(T)$, for dimensionless group adjusted in function on the pipe slope.

3.2. Sewer Pump Station Prototype Field Measurements

Prototype and model measurements are used together by assuming the predominant terms in Momentum equation are the inertial and gravity forces. Therefore, Froude similitude criterion is used. This hypothesis is evaluated hereinafter by comparing estimated and measured DO in the force main. Length ratio between prototype and ratio is given by:

$$L_{ratio} = \frac{L_{prototype}}{L_{model}} \approx \frac{700}{70} = 10 \quad (16)$$

Froude similitude criterion leads to the following velocity and flow rate ratios:

$$V_{ratio} = \frac{V_{prototype}}{V_{model}} = L_{ratio}^{0.5} = 3.16 \quad (17)$$

$$Q_{ratio} = \frac{Q_{prototype}}{Q_{model}} = L_{ratio}^{2.5} = 316 \quad (18)$$

Equations (16)–(18) are used for established the model water flow rate, so that Froude number of the model and prototype are equal, and therefore the other ratios can be used for estimate prototype variables from model ones.

Particularly, the depth of water flow inside the prototype pipe, h_f , can be calculated from Equation (16) and from model depth shown in Figure 11a. Thus, when the prototype flow rate is around $Q_W = 1200 \text{ m}^3/\text{h}$, water depth can be estimated at 0.46 and 0.35 m for a 1% and a 4% slope, respectively.

Figures 15–17 show measurements of several days in the force main with a water flow rate of $1200 \text{ m}^3/\text{h}$ when wastewater pumps are working, and with a continuous airflow rate of $240 \text{ m}^3/\text{h}$ (normal conditions) in the K.P. 0 + 800 and in the K.P. 1 + 300, with a 1% and a 4% slope, respectively. Moreover, H_2S in the discharge manhole, K.P. 1 + 500, was also measured and it is included in these figures.

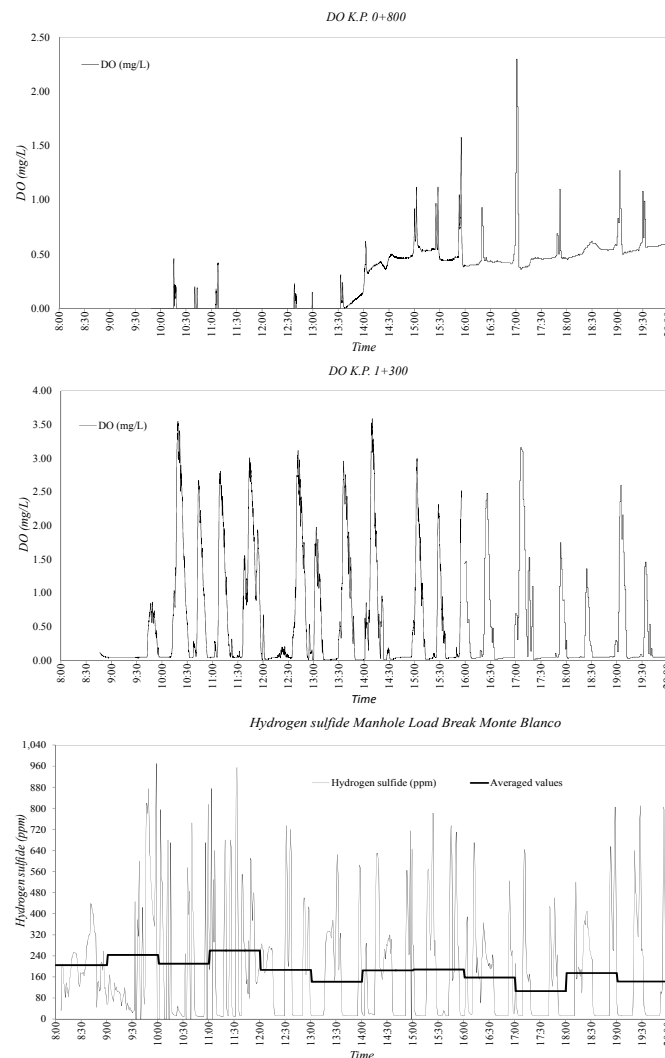


Figure 15. DO (mg/L) at K.P. 0 + 800 and 1 + 300 and H_2S (ppm) at the atmosphere of the manhole of discharge at K.P. 1 + 300 at 27 August 2014.

Figure 15 shows that, even though the air injection complies with previous advice, it is not effective. Actually, H_2S concentration on the discharge manhole reaches quite high values such as

1000 ppm, and on average is around 160 ppm. This verifies that dissolved sulfides are not disappearing. Besides DO in wastewater only reaches values over 1 mg/L when sewer station is pumping. Increase of DO is produced when pumps are working and decreases after pump stops. Pumps are working around 15 minutes each hour. Main differences between DO in K.P. 1 + 800 and 1 + 300 are due to force slope, which supposes different water level and values of inter-phase mass transfer and turbulent diffusivity. The multi-parameter probe at K.P. 0 + 800 is 0.16 m below water surface, while in K.P. 1 + 300 is 0.057 m below, which also influences in measured DO.

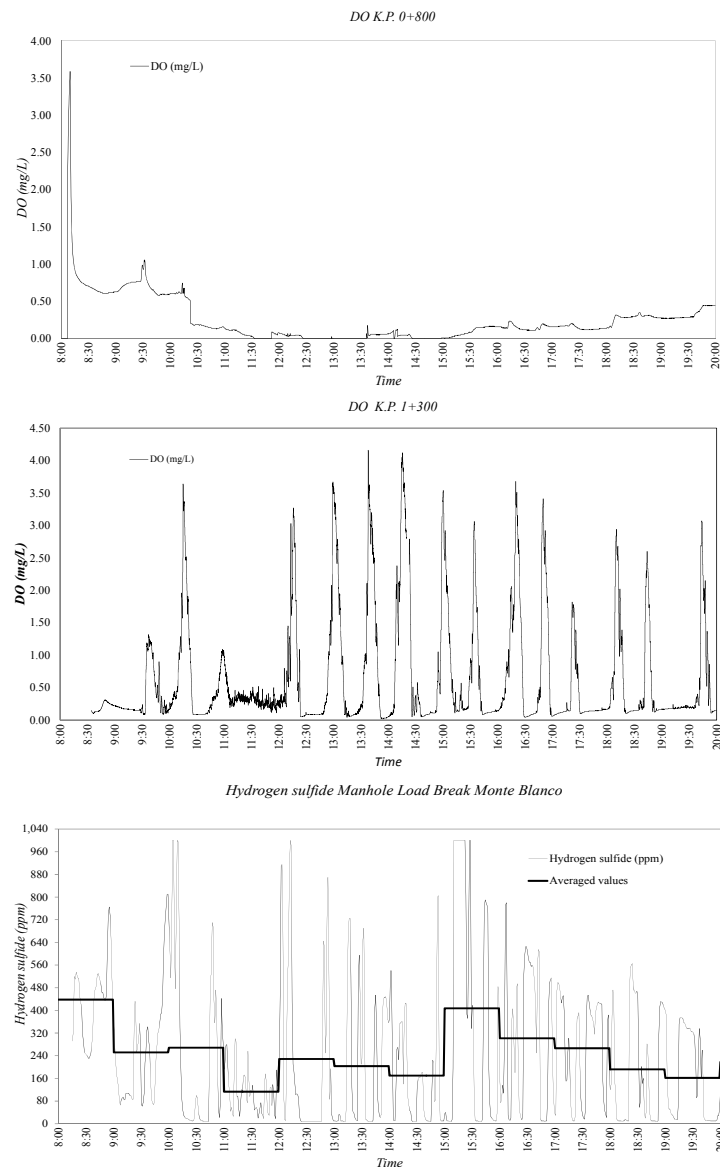


Figure 16. DO (mg/L) at K.P. 0 + 800 and 1 + 300 and H₂S (ppm) at the atmosphere of the manhole of discharge at K.P. 1 + 300 at 1 September 2014.

Figure 16 shows similar behavior to the previous figure. DO in the K.P. 1 + 300 reaches values of 2.0–4 mg/L while pumps were working, decreasing suddenly to zero due to DO consumption by organic matter degradation. From these drops the rate of DO consumption in the wastewater can be calculated in the range of 15 to 22 mg/L/h. In the case of K.P. 0 + 800 where multi-parameter probe is deeper, it is not observed that DO increase reflecting that diffusion of oxygen-transfer decreases with depth. Figure 16 shows that air injection treatment, due to insufficient transference of oxygen,

does not avoid sulfide generation either. Besides, air injected might favors sulfide release making it counterproductive in this force main, as is explained below.

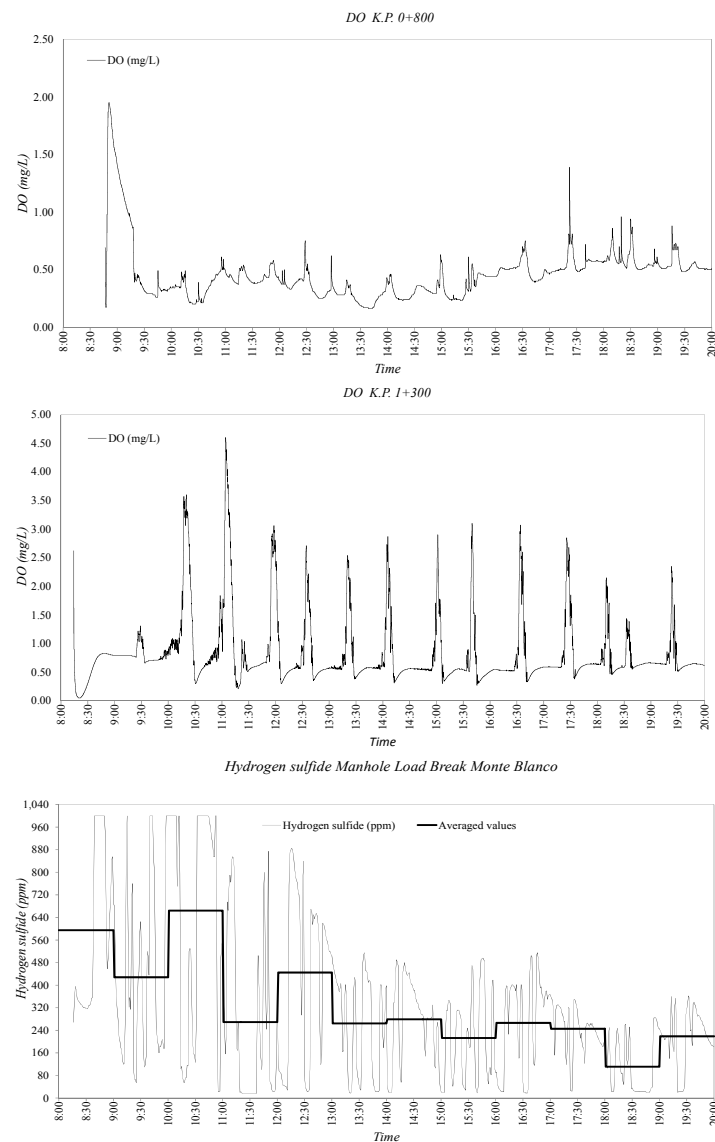


Figure 17. DO (mg/L) at K.P. 0 + 800 and 1 + 300 and H₂S (ppm) at the atmosphere of the manhole of discharge at K.P. 1 + 500 at 10 September 2014

As previously, Figure 17 confirms the inefficiency of the treatment in this force main. Averaged concentrations of H₂S at the discharge manhole are around 180 mg/L. As day passes, DO values around 0.5 mg/L are observed in the K.P. 0 + 800 multi-parameter probe. This is due to an increase of dissolved oxygen in the wastewater arriving to the pump station, as COD concentration is lower due to decrease in population.

As it was commented, injected air improves mixture between wastewater and air. This increases the mass transfer between air and water, e.g., the transfer of oxygen towards the water or the transfer of dissolved gases such as sulfides towards the air. Hence, the air injection tends to avoid sulfide generation by increasing DO in the water.

However, in this studied case, the quantity of oxygen being transferred is not enough to avoid sulfide generation. In this specific case, air injection can increase sulfide release. For a better understanding of this fact, we have included Figure 18, with measurements in the prototype in

a day in which no air was injected. It is observed that mean values of H₂S on days with no air injection are, on occasions, lower than those values on days with air injection, as seen in Figures 16 and 17.

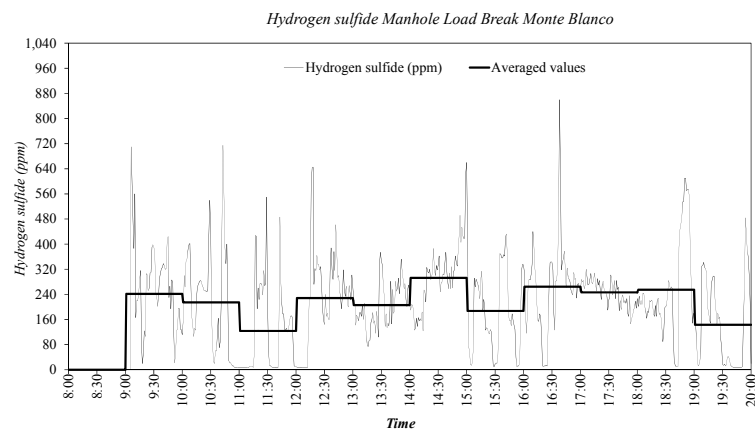


Figure 18. H₂S (ppm) at the atmosphere of the manhole of discharge at K.P. 1 + 500 at 26 August 2014.

3.3. Dissolved Oxygen Prediction. Second Fick's Law Application

In order to compare the results with probe measures, estimating the distribution of dissolved oxygen (DO) within a transversal section is needed. Indeed, parting from the variables calculated from experimental measurements in laboratory scale model such as turbulent diffusivity, E_m , and inter-phase mass transfer, $K_L(T)$, DO can be calculated at a certain position through the second Fick's law in a transversal section [18,19]:

$$\frac{\partial C}{\partial t} = D \frac{\partial^2 C}{\partial y^2} - (k_1 C + k_2) \quad (19)$$

where the boundary conditions are given by

$$y = 0 \rightarrow J = K_L(T)(C_{sat} - C) \quad (20)$$

$$y = h_f \rightarrow J = 0 \quad (21)$$

where y is the vertical coordinate in the transversal section (see Figure 5a), C the concentration of dissolved oxygen (DO) in a transversal section of a pipe in the coordinate y and the instant t (mg/L), while k_1 and k_2 are the constants of reaction, i.e., the rate of the oxygen used for organic matter oxidation. The constants k_1 and k_2 are coefficients that come from linear adjustment between the Oxygen Uptake Rate (OUR) and the DO concentration at the studied point. The OUR is the oxygen consumption expressed in mg/L/h units, and is calculated from slope of the descending part of the DO measurement curve registered by probes in prototype. At present work, DO consumption is within the range from 15 to 22 mg/L/h (Figures 15–17). Thus, oxygen consumption constants in Equation (19) are adjusted to $k_1 = 1.08 \times 10^{-5}$ (1/s) and $k_2 = 5.93 \times 10^{-3}$ (mg/L/s), in agreement with the suggested values by [1]. D is the sum of molecular and turbulent diffusivity, which can be considered equal to the turbulent diffusivity, $D \approx E_m$, given the higher value of turbulent diffusivity. A finite difference scheme is applied to solve second's Fick law:

$$C_{t+1}^i = C_t^i + \Delta t \left[D \frac{(C_t^{i+1} - 2C_t^i + C_t^{i-1}))}{\Delta y^2} - (k_1 C_t^i + k_2) \right] \quad (22)$$

$$y = 0 \rightarrow C_{t+1}^0 = C_t^0 + \frac{\Delta t}{\Delta y} \left[k(C_{sat} - C_t^0) \frac{S}{V} - D \frac{(C_t^0 - C_t^1)}{\Delta y} - (k_1 C_t^0 + k_2) \right] \quad (23)$$

$$y = h_f \rightarrow J = 0 \rightarrow \frac{\partial C}{\partial y} = 0 \rightarrow C_t^{h_f} = C_t^{h_f - \Delta y} \quad (24)$$

where $i = 1$ to n where $n = h_f / \Delta y$, with $\Delta y = 0.05$ m; $\Delta t = 0.1$ s; C_{sat} is the saturation concentration of oxygen in wastewater for the temperature and pressure of calculation (mg/L). S is the liquid—gas surface area (m²). V volume of wastewater (m³). From Equations (9), (13) and (14), values of E_m and $K_L(T)$ are calculated, respectively. Froude similitude is used to convert values to prototype so that they can be compared with DO multi-parameter probe measurements. Values used to solve second Fick's law are presented in Table 3. In this table probe position referred to water surface in presented according to Figure 5a. Figures 19 and 20 show solution of Equations (22)–(24) for the water flow rate of 1200 m³/h when pumps are working, and continuous airflow rate of 240 m³/h (normal conditions) at the positions where probes are located.

Table 3. Values of E_m and $K_L(T)$ adopted.

Case	E_m (m ² /s)	$K_L(28)$ (m/s)	$d_p = h_f - 0.3$ (m)
K.P. 0 + 800; $Q_w = 1200$ (m ³ /h); $Q_a = 240$ (m ³ /h); $i = 1\%$	9.92×10^{-5}	3.86×10^{-5}	0.161
K.P. 0 + 800; $Q_w = 0$ (m ³ /h); $Q_a = 240$ (m ³ /h); $i = 1\%$	6.32×10^{-5}	2.21×10^{-6}	0.127
K.P. 1 + 300; $Q_w = 1200$ (m ³ /h); $Q_a = 240$ (m ³ /h); $i = 4\%$	1.31×10^{-4}	6.41×10^{-5}	0.057
K.P. 1 + 300; $Q_w = 0$ (m ³ /h); $Q_a = 240$ (m ³ /h); $i = 4\%$	9.48×10^{-5}	9.48×10^{-6}	0.030

Calculated dissolved oxygen is compared with measured values showing a good agreement. Figures 19 and 20 show the evolution of DO from 09:50:24 to 11:16:48 during 27 August 2014 for the two points where the multiparametric probes are located. It can be shown that, during this period, the sewer pump has two active cycles. It is verified that DO decreases swiftly when pump stops.

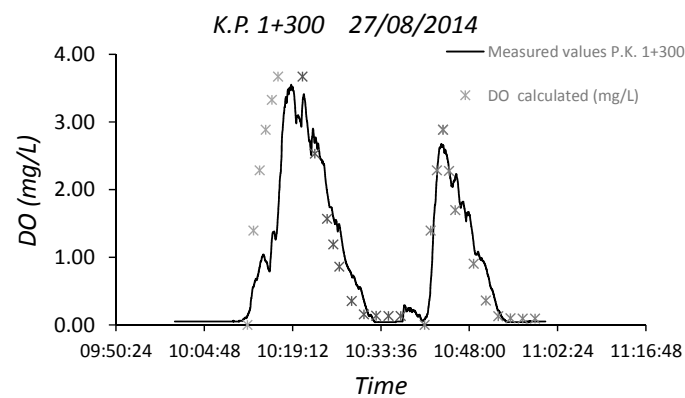


Figure 19. DO calculated and measured on 27 August 2014. Multi-parameter probe located at K.P. 1 + 300.

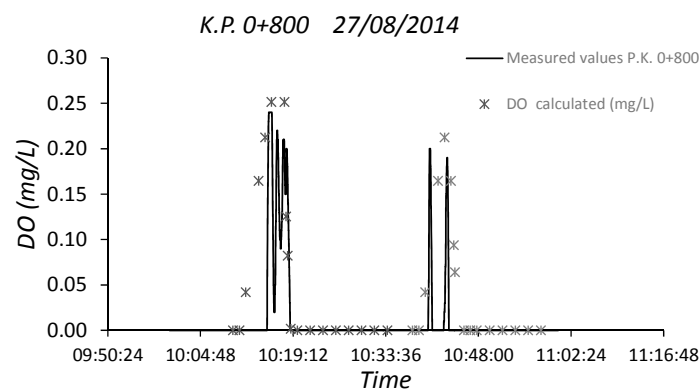


Figure 20. DO calculated and measured on 27 August 2014. Multi-parameter probe located at K.P. 0 + 800.

For a better understanding of the methodology proposed to calculate dissolved oxygen in wastewater in a force main a scheme of the steps followed is included at Figure 21.

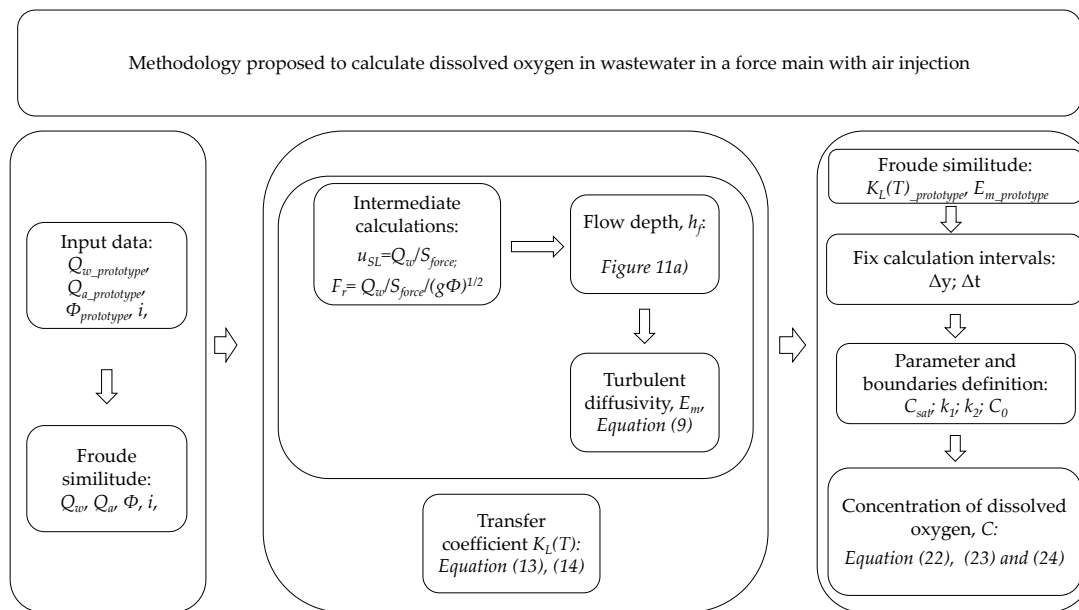


Figure 21. Scheme of methodology proposed to calculate dissolved oxygen in wastewater in a force main with air injection.

4. Conclusions

Measurements of two multi-parameter probes, located at two different positions in a force main, show an inefficient transfer of oxygen from injected air to wastewater (Figures 15–17), even if the chosen air–water flow ratio is higher than the highest from those suggested in the literature (Figure 1). In addition, high rates of hydrogen sulfide gas ($\text{H}_2\text{S}_{\text{atm}}$) are found at the discharge manhole of the main. For that reason, a scale model is constructed to study oxygen transfer to wastewater. Interphase mass transfer, $K_L(T)$, and turbulent diffusivity, E_m , are obtained from velocity field measurement in the pipe. These variables are defined for different slopes, and water and airflow rates. Results show an important influence of the pipe slope, resulting in important increases of oxygen transfer for 4% slopes compared to 1% slopes, as shown in Figure 13 and Equation (9). Water flow rate becomes an important variable whose increase also results in larger oxygen transfer. Diameter is also relevant as is proportional to the ratio between volume and surface air–water area, which indicates volume to consume the transferred oxygen. Airflow rate is relevant in the mass transfer and, even though it is not as relevant as water flow rate, its influence has to be considered.

Observed Flow is an elongated bubble flow in which oxygen transfer is produced basically at the front and back part of bubbles (Figures 8 and 9). Therefore, transfer increases with frequency of bubbles that is proportional to slope, i.e., adopting shorter lengths with slope increase (Figure 10a). Froude similitude is used to convert variables to prototype and second Fick’s law is solved to define oxygen transfer to water. From experiments and measurements, a procedure to calculate oxygen transfer, from air injection, into wastewater is proposed. Present methodology, from experimental measurements in a scale model, can constitute an adequate tool for the design of air injection into force mains. In fact, results of DO are compared with measurements showing good agreement. Thus, it is concluded that proposed methodology can quantify oxygen transfer into water.

Acknowledgments: The authors are grateful for the financial support received from Entidad de Saneamiento de la Región de Murcia (ESAMUR) and HIDROGEA through project: “Estudio en prototipo de inyección de aire en impulsiones de aguas residuales urbanas para la eliminación de olores”.

Author Contributions: Juan T. Garcia, Antonio Viguera-Rodriguez, Luis G. Castillo and Jose M. Carrillo carried out the direction, analysis and planning of laboratory tests and field measurements, analyzed the results and participated in written works.

Conflicts of Interest: The authors declare no conflict of interest.

Appendix A

Formulations to calculate inter-phase mass transfer from lab measurements [18,19].

Table A1. Formulae used to calculate inter-phase mass transfer coefficient.

Author Reference	Equation	Parameter Evaluated
Chu and Jirka (2003) [20]	$K_{Lw} = 2.150 \left(\frac{u_{*b}^3}{h_f} \right)^{0.25};$ $u_{*b} = \sqrt{f_f \left(\frac{ u_f u_f}{2} \right)};$ $K_{Lair} = 1.83 \times 10^{-3} u_{*a}^2$ $u_{*a} = \sqrt{f_i \left[\frac{\rho_{air} u_G - u_f (u_G - u_f)}{2} \right]} / \rho_{air}.$	K_{Lw} interphase mass transfer due to water flow (m/day); u_{*b} shear (friction) velocity of water flow (m/s); h_f flow depth in bubble zone (m); f_f is the Darcy–Weisbach friction factor of water flow and pipe (-); u_f is the velocity of the flow under the bubble (m/s) as seen in Figure 3; K_{Lair} interphase mass transfer due to airflow (m/day); u_{*a} shear (friction) velocity of airflow (m/s); f_i is the Darcy–Weisbach friction factor of air–water flow (-); u_G mean velocity of the air inside the bubble (m/s);
Guilliver et al. (1990) [21]	$K_{Lbubble} = 4.09 \frac{\alpha'_s}{\bar{d}_v} \frac{(1 - \alpha'_{air})^{1/2}}{(1 - \alpha'_{air})^{5/3}} \frac{D_{O_2-H_2O}^{1/2} (u-u)^{3/4}}{(\Phi v)^{1/4}}$ $D_{O_2-H_2O} = 7.4 \times 10^{-8} \frac{T(\Psi_{H_2O} M_{H_2O})^{1/2}}{\mu V_{O_2}};$ $\bar{d}_v = 0.299 \left(\frac{\sigma}{\rho} \right)^{3/5} \varepsilon^{2/5}; \varepsilon = \frac{((u_{*b})^2)^{3/2}}{0.07 h_f};$ $\alpha_{air} = 1 - \frac{1}{1 + (\frac{u_s}{8.66})^{1.39}}; \alpha'_{air} = \alpha_{air} \frac{l_{mixture}}{l_{slug}}$	$K_{Lbubble}$ due to mixture (m/day); $D_{O_2-H_2O}$ turbulent diffusivity in the water flow (m ² /s); T = temperature (°K); $\Psi_{H_2O} = 2.26$; M_{H_2O} = molecular weight of water = 18 g/mol; μ = dynamic viscosity of water 0.890 (cP); V_{O_2} = Molar volume of oxygen 25.6 cm ³ /g-mol; σ = surface tension of water 0.0728 kg/s ² ; \bar{d}_v bubble medium diameter; ε rate of turbulent kinetic energy dissipation per unit mass; α_{air} and α'_{air} fraction of air in the slug and in the mixture zone respectively.
Measured at present work	$l_{mixture} = 2.7 \Phi \sqrt{F_{r2}^2}$	$l_{mixture}$ of bubbles in the slug flow adjusted from observations (m); Φ inner diameter of pipe; F_{r2}^2 square Froude number Equation (1) adapted from [22].

References

- Hvitved-Jacobsen, T.; Vollertsen, J.; Nielsen, A.H. *Sewer Processes: Microbial and Chemical Process Engineering of Sewer Networks*; CRC Press: Boca Raton, FL, USA, 2013.
- Zhang, L.; De Schryver, P.; De Gussemé, B.; De Muynck, W.; Boon, N.; Verstraete, W. Chemical and biological technologies for hydrogen sulfide emission control in sewer systems: A review. *Water Res.* **2008**, *42*, 1–12. [CrossRef] [PubMed]
- Pomeroy, R. Generation and control of sulfide in filled pipes. *Sew. Ind. Wastes* **1959**, *31*, 1082–1095.
- Sewell, R.J. *Controlling Sulfides in Sanitary Sewers Using Air and Oxygen*; National Environmental Research Center: Cincinnati, OH, USA, 1975.
- Design Manual. *Odor and Corrosion Control in Sanitary Sewerage Systems and Treatment Plants*; Center for Environmental Research Information, US Environmental Protection Agency, Office of Research and Development: Washington, DC, USA, 1985.
- Tanaka, N.; Takenaka, K. Control of hydrogen sulfide and degradation of organic matter by air injection into a wastewater force main. *Water Sci. Technol.* **1995**, *31*, 273–282. [CrossRef]
- Kameda, Y.; Morita, T. Two-phase flow study using 300 mm diameter pipe. *Jpn. J. Multiph. Flow* **1990**, *4*, 219–249. [CrossRef]

8. Kameda, Y.; Morita, T. Two-phase flow study using 200 mm diameter pipe. *Jpn. J. Multiph. Flow* **1993**, *7*, 250–261. [[CrossRef](#)]
9. Ochi, T.; Kitagawa, M.; Tanaka, S. Controlling sulfide generation in force mains by air injection. *Water Sci. Technol.* **1998**, *37*, 87–95. [[CrossRef](#)]
10. Tanaka, N.; Hvitved-Jacobsen, T.; Ochi, T.; Sato, N. Aerobic-Anaerobic Microbial Wastewater Transformations and Re-aeration in an Air-Injected Pressure Sewer. *Water Environ. Res.* **2000**, *72*, 665–674. [[CrossRef](#)]
11. Taitel, Y.; Dvora, B. Two-phase slug flow. *Adv. Heat Transf.* **1990**, *20*, 83–132.
12. Hanratty, T.J. *Physics of Gas-Liquid Flows*; Cambridge University Press: Cambridge, UK, 2013.
13. Lauchlan, C.S.; Escarameia, M.; May, R.W.P.; Burrows, R.; Gahan, C. *Air in Pipelines*; Report SR; HR Wallingford: Wallingford, UK, 2005; p. 649.
14. Barnea, D.; Shoham, O.; Taitel, Y.; Dukler, A.E. Flow pattern transition for gas-liquid flow in horizontal and inclined pipes. Comparison of experimental data with theory. *Int. J. Multiph. Flow* **1980**, *6*, 217–225. [[CrossRef](#)]
15. Adrian, R.J.; Westerweel, J. *Particle Image Velocimetry*; Cambridge University Press: Cambridge, UK, 2010; ISBN: 9780521440080.
16. Thielicke, W.; Stamhuis, E.J. PIVlab—Time-Resolved Digital Particle Image Velocimetry Tool for MATLAB. Version 1.4. 2014. Available online: <http://dx.doi.org/10.6084/m9.figshare.1092508> (accessed on 28 February 2017).
17. Socolofsky, S.A.; Jirka, G.H. *Environmental Fluid Mechanics 1: Mixing and Transport Processes in the Environment*; Texas A and M University: College Station, TX, USA, 2005.
18. Crank, J. *Mathematics of Diffusion*, 2nd ed.; Clarendon Press: Oxford, UK, 1975.
19. Pai, T.Y.; Ouyang, C.F.; Liao, Y.C.; Leu, H.G. Oxygen transfer in gravity flow sewers. *Water Sci. Technol.* **2000**, *42*, 417–422.
20. Chu, C.R.; Jirka, G.H. Wind and stream flow induced reaeration. *J. Environ. Eng.* **2003**, *129*, 1129–1136. [[CrossRef](#)]
21. Gulliver, J.S.; Thene, J.R.; Rindels, A.J. Indexing gas transfer in self-aerated flows. *J. Environ. Eng.* **1990**, *116*, 503–523. [[CrossRef](#)]
22. Hager, W.H. *Energy Dissipators and Hydraulic Jump*; Springer Science & Business Media: Berlin, Germany, 2013; Volume 8.



© 2017 by the authors. Licensee MDPI, Basel, Switzerland. This article is an open access article distributed under the terms and conditions of the Creative Commons Attribution (CC BY) license (<http://creativecommons.org/licenses/by/4.0/>).